[CANCER RESEARCH 63, 8256–8263, December 1, 2003] Exhibit 6

Inducible Prostate Intraepithelial Neoplasia with Reversible Hyperplasia in Conditional FGFR1-Expressing Mice

Kevin W. Freeman,[1,2] Bryan E. Welm,[2,3] Rama D. Gangula,[1] Jeffrey M. Rosen,[2,3] Michael Ittmann,[4] Norman M. Greenberg,[2,3] and David M. Spencer[1,2]

[1]Department of Immunology, [2]Program in Cell and Molecular Biology, [3]Department of Molecular and Cellular Biology, and [4]Department of Pathology, Baylor College of Medicine, Houston, Texas

ABSTRACT

Accurate determination of the contributions of oncogenes toward tumor progression requires their regulation. Herein, we created transgenic mice with prostate-specific expression of ligand-inducible FGFR1 or FGFR2, based on lipid-permeable dimerizing molecules, called chemical inducers of dimerization. Despite extensive homology and equivalent expression by both chimeric receptors in the ventral prostate gland, only FGFR1 triggers detectable nuclear translocation of Erk and progression to prostatic intraepithelial neoplasia (PIN). Induction of PIN grade I-II, indicated by multiple layers of atypical cells, is seen consistently by 12 weeks of chemical inducers of dimerization treatment. By 6 months, more extensive nuclear atypia, thickened "reactive" stroma, and basement membrane herniation occurs, corresponding to PIN IV. By timed removal of FGFR1 signaling, we show that induced hyperplasia is reversible until extensive intraductal vascularization occurs, but continued progression requires prolonged FGFR1 signaling. Additionally, by highlighting differences between the two receptors and creating the foundation for controlling FGFR1 signaling during prostate cancer progression, a model of early stage prostate cancer is established for developing targeted intervention directed toward the FGFR signaling axis.

INTRODUCTION

Despite improvements in the management of organ-confined disease, CaP[5] will claim ~30,000 lives in the United States in 2003 (1), largely due to the absence of effective treatment for metastatic disease. More accurate modeling of CaP is required to better understand the molecular signaling events and pathological stages associated with disease progression, and to facilitate development of more effective therapeutics. Several mouse models of CaP have been developed previously (2). These models fall into two broad categories, the more aggressive SV40 T antigen-based models, such as TRAMP (3) or "Lady" (4) that target multiple tumor suppressor genes, and a variety of other less aggressive models that target a single proto-oncogene or tumor suppressor molecule, such as FGF-8 (5) or PTEN (6). Whereas the single-gene models tend to highlight the early stages of progression, TRAMP mice consistently develop metastatic CaP by 28 weeks of age, allowing for therapeutic studies that span a relatively short time (7, 8). Whereas both sets of models can help determine genetic lesions capable of contributing to disease, neither permits temporal ordering of deleterious genetic events or highlights whether those genetic changes only initiate disease or are also required for disease maintenance, and may, therefore, be targeted for therapeutic intervention.

To achieve temporal control of the FGFR axis implicated in early changes associated with CaP (9) we used CID technology, which allows rapid activation of target proteins, such as growth factor receptors, that are naturally activated by oligomerization (10). CID-inducible growth factor receptors are engineered by substituting the ligand-binding extracellular domain of the receptor with a cytoplasm-localized drug-binding domain (*e.g.,* FKBP12 variants), which, on binding of a lipid-permeable dimeric drug (*e.g.,* AP20187), causes receptor oligomerization, transphosphorylation, and activation of downstream signaling cascades (11–14). Because the investigator dictates the schedule of AP20187 administration, temporal control in the activation and inactivation of the receptor is possible, highlighting the pathological features dependent on the growth factor receptor for both initiation and maintenance of phenotype. Additionally, unlike bigenic transcription switch (*e.g.,* tet) -regulatable systems or conditional lesions based on recombination (*e.g.,* Cre/lox), this approach requires only a single transgenic change, greatly simplifying breeding strategies.

In the currently accepted model of FGF signaling in the normal prostate, stromal-derived FGF7/keratinocyte growth factor and FGF10 help maintain epithelial differentiation and survival through glandular epithelium-confined FGFR2-IIIb, contributing to epithelial dependence on the stroma. During progression to malignancy, the observed molecular changes in the FGF signaling axis that occur in the epithelium include loss of normal FGFR2 signaling (by isoform changes that alter ligand binding or by loss of FGFR2 expression), acquisition of FGFR1 expression, and up-regulation of distinct FGF family members. These changes likely allow autocrine signaling via FGFR1 and possibly FGFR2, permitting independence from stromal-derived FGFs and, thus, deregulated growth of the epithelium (9, 15). In addition to observed changes in CaP, these alterations are common in bladder and salivary adenocarcinomas, where up-regulation of FGFR1 is associated with tumor progression, and ectopic expression of FGFR2 inhibits progression and growth of transplanted tumors (16, 17). Despite accumulating data in model tumor systems, the effects of these two receptors have not been investigated before in a normal prostate epithelium, although overexpression of FGFs in the prostate has led to the development of prostatic hyperplasia and PIN (5, 18–20).

In this study we focused on the hyperplasia-stimulating effects of ectopic FGFR1 signaling on normal prostatic epithelium, demonstrating diverse effects of iFGFR1 and iFGFR2 in a normal prostate background, and showing dependence of hyperplasia and proliferation on continued iFGFR1 signaling. Whereas the profound hyperplasia that is seen after only 1 month of FGFR1 stimulation is completely reversible, neovascularization, which is well established by 2 months, is associated with hyperplastic cells becoming largely independent of iFGFR1 signaling for their survival. Moreover, moderate-term (*i.e.,* <6 months) iFGFR1 signaling can promote high-grade (*i.e.,* type IV) PIN that is associated with a thickened stroma, fulminant glandular hyperplasia, nuclear atypia, and basement membrane herniation. This

Received 5/22/03; revised 9/11/03; accepted 9/18/03.

Grant support: NIH Grants R01-CA87569, UO1-CA84296, and T32-AI07495 (K. W. F.).

The costs of publication of this article were defrayed in part by the payment of page charges. This article must therefore be hereby marked *advertisement* in accordance with 18 U.S.C. Section 1734 solely to indicate this fact.

Notes: Dr. Welm is currently in the Department of Anatomy, University of California, San Francisco, California.

Requests for reprints: David M. Spencer, Baylor College of Medicine, One Baylor Plaza/M929, Houston, TX 77030. Phone: (713) 798-6475; Fax: (713) 798-3033; E-mail: dspencer@bcm.tmc.edu.

[5] Abbreviations: CaP, cancer of the prostate; CID, chemically induced dimerization; HA, hemagglutinin; FGF, fibroblast growth factor; FGFR, fibroblast growth factor receptor; iFGFR, inducible fibroblast growth factor receptor; PIN, prostatic intraepithelial neoplasia; TRAMP, transgenic adenocarcinoma of the mouse prostate; JOCK, juxtaposition of CID and Kinase-1; p, phospho.

Exhibit 6

is the first reported example of a conditionally reversible CaP model, and the first study of the diverse effects of FGFR1 and FGFR2 signaling in the context of a normal mouse prostate.

MATERIALS AND METHODS

Construction of Transgene. The plasmid construct pSH1/M-FGFR2-F_vF_{vls}-E was created by PCR amplifying the cytoplasmic domain of FGFR2 using forward primer 5′-AATTAACTCGAGGACTTCAGCAGCCAGC-CAGCT-3′ and reverse primer 5′-AGTTCAGTCGACTGTTTTAACACTGC-CGTTTATGTGTG-3′, following the same procedure for making pSH1/M-FGFR1-F_vF_{vls}-E as described previously (21). Briefly, the cytoplasmic signaling domains of FGFR1 and FGFR2 were PCR amplified with *Xho*I and *Sal*I flanking sites, and cloned into parent expression vector pSH1/M-F_v-F_{vls}-E (22). The *Xba*I-*Bam*HI fragment of the ARR_2PB promoter was subcloned into the *Cla*I-*Bam*HI site of expression vector, KBPA, to create ARR_2PB-KBPA. The *Not*I-*Mun*I fragments from pSH1/M-FGFR1-F_vF_{vls}-E and pSH1/M-FGFR2-F_vF_{vls}-E were subcloned into the *Eco*RI site of ARR_2PB-KBPA to create ARR_2PB-KBPA-iFGFR1 and ARR_2PB-KBPA-iFGFR2. Both transgene constructs were cleaved with *Not*I and *Kpn*I, and fragments were isolated by agarose gel and purified by Qiagen (Valencia, CA) spin columns for injection into FVB strain-derived embryonic stem cells.

Mice and Reagents. All of the mice were FVB (bred in-house) background and kept pathogen free in the Texas Mouse Facility under veterinary supervision. AP20187 was dissolved in 16.7% propanediol, 22.5% PEG400, 1.25% Tween 80 and injected i.p. biweekly at 2 mg/kg. On the basis of an estimated half-life *in vivo* of 7 h[6] and an EC_{50} *in vitro* of ~10 nM (data not shown), this level was calculated to evoke signaling for 2–3 days *in vivo*. Alternatively, carrier alone was injected. Initiation of treatments was staggered so that all of the mice were the same age when prostates were harvested.

Immunoprecipitation and Western Blot Analysis. Organs were harvested, frozen, pulverized, and then lysed in 200–300 μl of radioimmunoprecipitation assay buffer [0.01 M Tris-CL (pH 8.0), 0.14 M NaCl, 1% Triton X-100, 1% sodium deoxycholate, and 0.1% SDS] with 1 mM phenylmethylsulfonyl fluoride and protease inhibitor mixture (Sigma-Aldrich, St. Louis, MO) and incubated on ice for 2 h. SDS-PAGE was performed as described previously (22). Membranes were incubated with primary antibody HA.11 (Covance, Richmond, CA) at 1:1500 or α-tubulin (Santa Cruz Biotechnology, Santa Cruz, CA) diluted 1:500 for 1 h and then with secondary horseradish peroxidase-linked polyclonal goat antimouse antibody (1:2000; Santa Cruz Biotechnology) for 30 min. Membranes were washed 3X with Tris-Buffered Saline plus 0.1% Tween-20 (TBST) for 5–15 min after each antibody step. Bands were visualized with SuperSignal chemiluminescence substrate (Pierce, Rockford, IL). Immunoprecipitation was carried out using the IMMUNOcatcher kit (Cytosignal Research Products, Irvine, CA) following the manufacturer's protocol using 2 μg antiphosphotyrosine antibody 4G10 (Upstate, Lake Placid, NY) for immunoprecipitation and HA.11 immunoblotting as above. Phosphatase inhibitor I and II (Sigma) were added to lysates.

Histology and Immunohistochemistry. Microdissected prostates were placed overnight in 10% neutral phosphate-buffered formalin, transferred to 50% neutral phosphate-buffered formalin/50% ethanol for 1 h and then 70% ethanol until paraffin embedding. After sectioning (5 μM) and mounting onto ProbeOn-Plus slides (Fisher, Pittsburgh, PA), slides were deparaffinized and hydrated with progressive xylene washes followed by a gradient of ethanol and PBS. Slides were either directly stained with H&E or immunostained. For antigen retrieval, slides were either placed into boiling 10 mM citric acid for 30 min and allowed to cool at 25°C or were proteinase K-treated. Both sets were quenched in 3% H_2O_2, blocked with Power Block (Biogenex Laboratories, San Ramon, CA) for 10 min at 25°C, and incubated with either anti-Ki-67 antibody (Novacastra, Newcastle upon Tyne, United Kingdom) at 1:1000, anti-CD31/PECAM (BD PharMingen, San Diego, CA) at 1:100, or anti-phospho-Erk (Cell Signaling Technology, Beverly, MA) at 1:100 in Power Block overnight at 4°C, followed by incubation with biotin-conjugated goat antirabbit antibody (Vector Laboratories, Burlingame, CA) at 1:2000 or goat antimouse biotin-conjugated antibody (Santa Cruz Biotechnology) at 1:100 for 1 h. After each incubation, slides were washed with PBS plus 0.1% Tween for 2 h. Immunostaining was visualized using the ABC kit (Vector Laboratories), and slides were counterstained with methyl green and dehydrated using a gradient of ethanol to xylene before mounting under coverslips.

[6] T. Clackson, personal communication.

RESULTS

Targeting Conditional FGFR1 and FGFR2 to the Prostate. In these studies iFGFR1 and iFGFR2 transgenes were placed under the transcriptional control of the prostate epithelium-targeted composite probasin promoter, ARR_2PB (23). The iFGFR constructs each contain an NH_2-terminal myristoylation-targeting signal sequence for membrane localization, followed by the intracellular signaling domains of FGFR1 or FGFR2, two-tandem AP20187 drug binding domains (F_v2) and a COOH-terminal HA epitope tag introduced into an expression vector, KBPA, backbone (Fig. 1*A*). FVB blastocysts were injected separately with both constructs, leading to two founder lines of iFGFR1, collectively named JOCK-1, and one founder line expressing iFGFR2, named JOCK-2. All three of the lines expressed detectable transgene by Western blotting of prostate tissue, and the highest expressing JOCK-1 line was chosen for additional study (data not shown). To determine the tissue-specificity of the transgenes, multiple organs from 12-week-old transgenic mice were homogenized, and tissue lysates were separated by SDS-PAGE followed by anti-HA immunoblotting. This analysis revealed that ARR_2PB-driven transgene expression was primarily prostate-specific, consistent with previous reports (Refs. 23, 24; Fig. 1*B*). Furthermore, to determine expression within the various distinct lobes of the murine prostate, microdissected anterior (coagulating gland), ventral, dorsal, and lateral lobes were also analyzed for specific transgene expression. In ventral lobes, relatively high-level transgene expression was comparable between JOCK-1 and JOCK-2, and in lateral and anterior lobes, weak but equivalent expression was also seen. However, significantly higher transgene expression was seen in the dorsal prostate of JOCK-2 (Fig. 1*C*). In both JOCK-1 and JOCK-2 mice, immunohistochemistry with antibodies to HA shows equivalent localization and transgene expression in the luminal epithelial cells of the ventral prostate (Fig. 1, *D* and *E*), as well as higher transgene expression in the luminal epithelial cells of the dorsal prostate of JOCK-2 mice (data not shown), matching the expression levels observed by anti-HA immunoblotting. Thus, due to high-level comparable transgene expression, we focused most comparative studies on the ventral prostate lobes of JOCK-1 and JOCK-2 mice.

FGFR1, but not FGFR2, Signaling Leads to Hyperplasia and Dysplasia. To determine the cumulative effects of iFGFR1 and iFGFR2 signaling, 12-week-old male JOCK mice were treated for a period of 1–12 weeks with biweekly i.p. injections of AP20187 (2 mg/kg), which should permit signaling in target prostate tissue for up to 2–3 days after CID administration (see "Materials and Methods"). After drug treatment, prostates were isolated, microdissected, fixed, and processed for histology. In JOCK-1 mice, after 2 weeks of AP20187 treatment, staining with H&E revealed development of low-grade PIN (type I and II; Ref. 25) in the ventral, dorsal-lateral, (Fig. 2, *C* and *D*), and anterior prostate (data not shown). In contrast, similarly treated JOCK-2 mice showed no obvious phenotypic changes in any lobe, including the ventral and dorsal-lateral prostate (Fig. 2, *E* and *F*), suggesting that these homologous receptors have fundamental differences. Furthermore, AP20187 had no effect on wild-type mice treated for 12 weeks (Fig. 2, *A* and *B*), consistent with Phase I clinical trials of AP20187 analogue, AP1903 (26).

Because no phenotype was observed in the JOCK-2 mice, tyrosine phosphorylation of the iFGFR2 was analyzed by immunoprecipitation with antiphosphotyrosine-specific antibodies and immunoblotting with antibodies specific to the HA epitope tag of iFGFR2. From

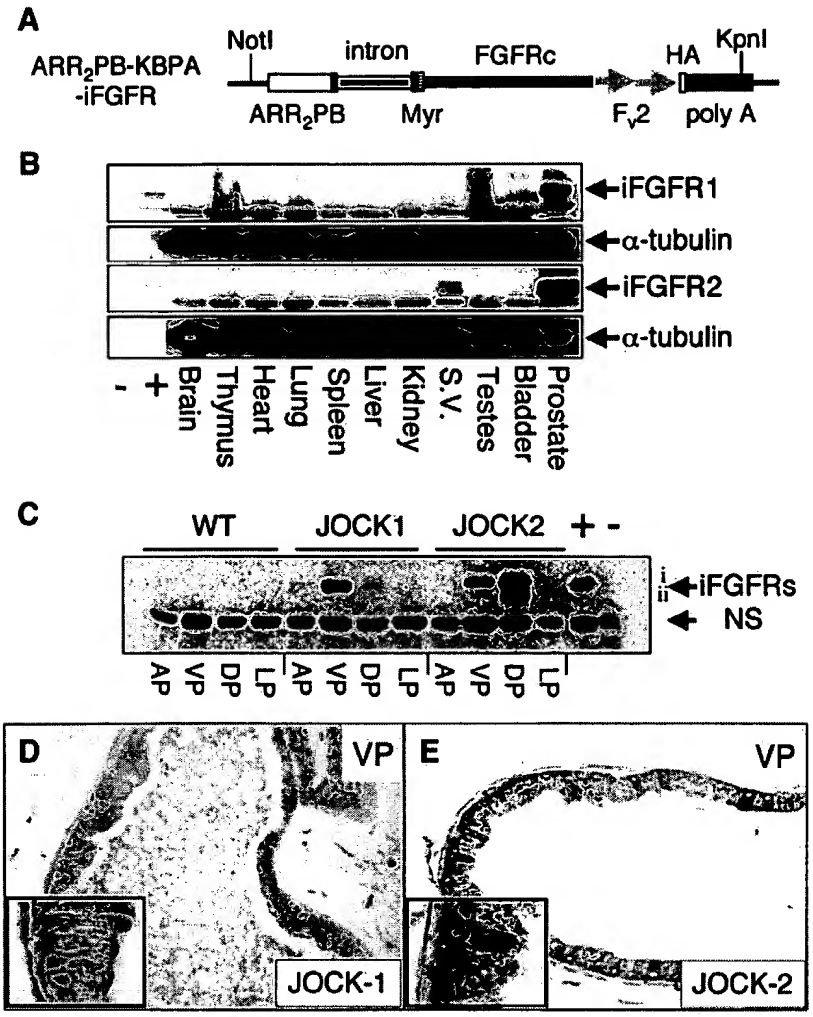

Fig. 1. Generation of inducible FGFR1 and FGFR2 mice. Schematic of iFGFR transgene construct showing the intracellular domain of either FGFR1 or FGFR2 (*FGFRc*), downstream of the myristoylation targeting sequence of v-Src (*Myr*) and upstream of two tandem AP20187-binding proteins (F_v2) and the HA epitope tag (*A*). Expression is regulated by the prostate-targeted promoter ARR_2PB, the KCR "intron," and the "poly(A)" sequence from the bovine growth hormone gene. *B* and *C*, Western blot analysis, using antibodies specific for the HA epitope of the iFGFRs (*B* and *C*) or α-tubulin (*B*), of lysates from various organs harvested from JOCK-1 and JOCK-2 mice (*B*), or of lysates from the anterior (*AP*), ventral (*VP*), dorsal (*DP*), or lateral (*LP*) lobes of the prostate (*i*) indicating full-length protein and (*ii*) indicating a degradation product (*C*). Both JOCK-1 and JOCK-2 mice display prostate-specific expression of the transgenes (*B*), with equivalent strong expression in the ventral prostate, equivalent weak expression in anterior and lateral lobes, and stronger dorsal expression in JOCK-2 mice (*C*). Paraffin sections from the ventral prostate of JOCK-1 and JOCK-2 mice immunostained with anti-HA for transgene expression (*D* and *E*). Panels originally at ×200 (*D* and *E*) and insets at ×400.

lysates of total prostate, we observed comparable CID-mediated receptor tyrosine phosphorylation 24 h after CID treatment for both JOCK-1 and JOCK-2 mice, verifying that iFGFR2 was functional (data not shown). Additional previous studies demonstrate that this receptor is functional in mammary epithelium (21) and TRAMP-derived cell lines (30). However, because transgene expression was variable between the different lobes of the prostates of JOCK-1 and JOCK-2 mice, we repeated the above experiment on individual prostate lobes. Although iFGFR1 tyrosine phosphorylation was observed in the ventral lobe of JOCK-1 mice, no receptor tyrosine phosphorylation was observed in the ventral lobe of JOCK-2 mice. Nevertheless, when lysates are immunoblotted for HA, we did observe a CID-induced shift in protein migration of iFGFR2, possibly due to Ser/Thr phosphorylation of the receptor (Fig. 2*G*). This suggests that iFGFR2 is activated in the ventral prostate, leading to direct or indirect modification. Also, phenotypic differences between the ventral prostates of CID-treated JOCK-2 mice *versus* JOCK-1 mice may still be due to quantitatively lower FGFR2 activation.

Because iFGFR2 tyrosine phosphorylation was observed in intact JOCK-2 prostates, we wanted to determine whether this phosphorylation was localized to the dorsal lobe where JOCK-2 mice show much higher transgene expression than JOCK-1 mice. As predicted, tyrosine phosphorylation of iFGFR2 was detected in the dorsal prostate (Fig. 2*H*). This suggests that FGFR2 activation is insufficient to induce phenotypic changes in the dorsal prostate after 12 weeks of CID treatment, whereas much lower levels of iFGFR1 are capable of driving the dorsal prostate to PIN II. This demonstrates for the first time that these two receptors can have broadly different effects on normal prostatic epithelial proliferation (Fig. 2, *C* and *D, versus* Fig. 2, *E* and *F*).

To determine the progressive effects of continuous (or semicontinuous) iFGFR1 signaling over time, we focused on phenotypic changes in the ventral lobe due to the consistent changes we observed in preliminary experiments. Within the first week of AP20187 treatment, increased vacuolization, a marker for increased metabolic activity, and modest hyperproliferation were already apparent (data not shown). From 2 to 4 weeks of CID treatment, JOCK-1 mice showed pronounced hyperproliferation in all lobes of the prostate. (Fig. 3*B*) By 8 weeks of AP20187 administration, iFGFR1 activation led to the establishment of extensive intraductal vascularization (Fig. 3*F*), which was not evident in hyperplastic acini at 4 weeks (Fig. 3*E*). Additionally, increased nuclear atypia, chromatin condensation, and formation of papillary structures were observed (Fig. 3, *C* and *F*). By 12 weeks of activation, mice were determined to have low-grade PIN in all of the lobes examined, characterized by epithelial "piling-up," elongated and hyperchromatic nuclei, and cribiform glandular structures (Fig. 3*D*), as well as stromal thickening in the dorsal lobes of some mice. Longer-term treatments of 24 and 30 weeks led to the widespread development of "reactive" thickened stroma (Fig. 3*J*). Additionally, more extensive dysplastic nuclei and herniated acini with extraglandular extension were observed at 24 (Fig. 3, *G* and *H*) and 30 weeks (Fig. 3*I*), consistent with grade IV PIN (25). As an

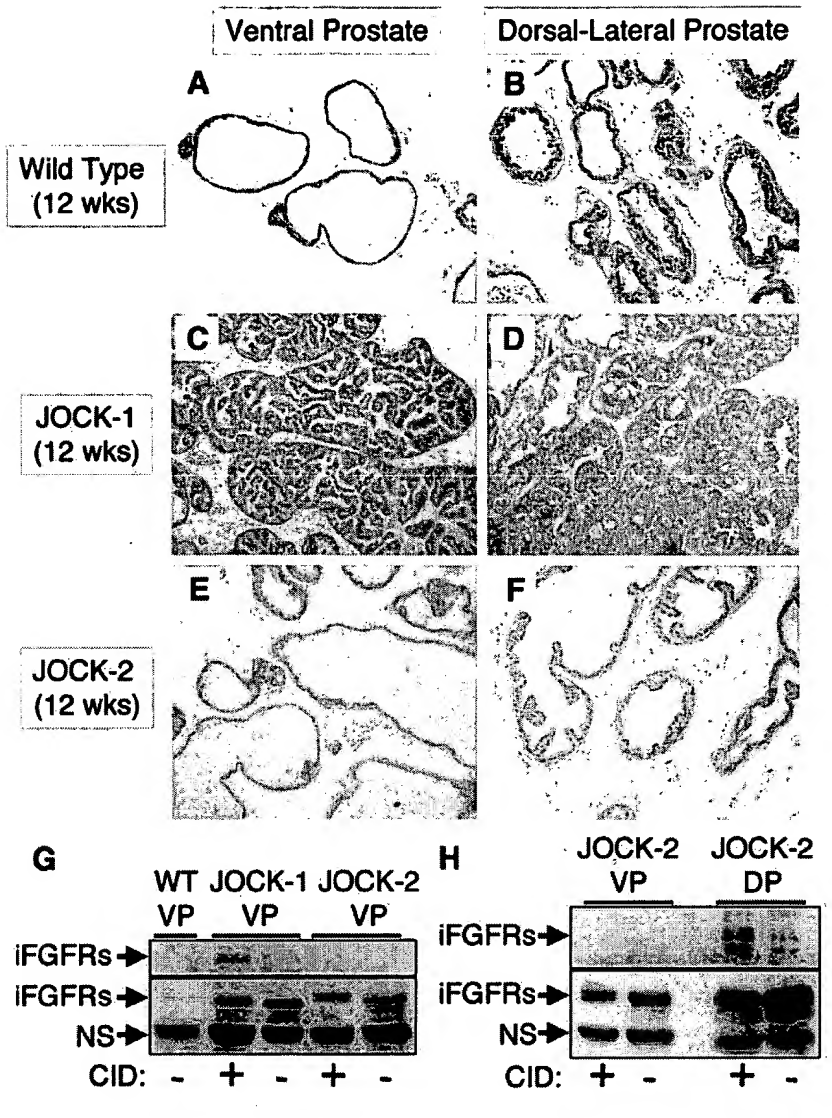

Fig. 2. Inducible FGFR1 but not iFGFR2 signaling leads to PIN in all lobes of the prostate. Wild-type mice (*A* and *B*), JOCK-1 mice (*C* and *D*), and JOCK-2 mice (*E* and *F*) were treated for 12 weeks with AP20187. Paraffin sections from the ventral (*VP*; *A, C,* and *E*) and dorsal-lateral (*DLP*; *B, D,* and *F*) prostate were H&E stained for morphological analysis. Panels at ×100 (*A–F*). JOCK-1 or JOCK-2 mice were treated with AP20187 24 h before the prostates were harvested, microdissected, and lysed for immunoprecipitation with antiphosphotyrosine antibodies, followed by immunoblotting with anti-HA (*top; G* and *H*). For loading control, 10% of the lysate was immunoblotted with anti-HA (*bottom; G* and *H*).

additional indication of PIN, we observed increases in cytokeratin-8 as early as 12 weeks of age with more profound increases appearing by 24 weeks (data not shown; Ref. 25). These results demonstrate iFGFR1-driven progression of normal epithelial cells to high-grade PIN and show a strong oncogenic effect of FGFR1 on normal prostate epithelium that is not shared by FGFR2.

Hyperplasia Is Reversible Until Neovascularization. In contrast to conditional genetics based on tissue-specific activation of dominant-negative or constitutive alleles (*e.g.*, using Cre/lox technology), a distinct feature of the JOCK model is the ability to remove signaling by withholding CID. After demonstrating the degree to which iFGFR1 signaling could alter normal prostate epithelial cells in <6 months, we wanted to determine at which stages of progression, if any, changes would become irreversible. Therefore, we first investigated the effects of CID withdrawal on the prostate after ~4 weeks of AP20187 treatment, which is before initiation of obvious intraepithelial vascularization. Mice were treated biweekly with CID for 4 weeks, and then AP20187 administration was terminated for various times up to 8 weeks. Although dramatic changes in proliferation were apparent within days (Fig. 5*A*), loss of supernumerary epithelial cells was gradual over the 8-week period, resulting in a prostate almost indistinguishable from untreated tissue (Fig. 4*A versus B*; data not shown). Thus, before extensive neovascularization, iFGFR1 signaling is required for maintenance of hyperplasia.

Because newly vascularized tissue might be able to support greater cellularity even in the absence of ectopic signaling, we wanted to determine whether later stages of hyperplasia associated with intraglandular vascularization were also reversible. Therefore, JOCK-1 mice were treated for 8 weeks with CID, when extensive intraglandular vascularization is consistently observed, and treatment was stopped for an additional 8 weeks before histological examination. In contrast to animals treated for only 4 weeks, we observed no loss of hyperplasia in the ventral prostate. (Fig. 4, *C versus D*) Although regression was not observed in the ventral prostate, there was a decrease in proliferation, and additional progression to low-grade PIN was not observed (Fig. 4, *E versus F;* data not shown). Thus, hyperplasia is reversible until established neovascularization, whereas prolonged iFGFR1 activation is required for continued proliferation and additional progression.

Increased Hyperplasia in JOCK-1 Is Driven Largely by Hyperproliferation. Because hyperplasia can be caused by increased proliferation or decreased apoptosis, we wanted to determine the contributions of both to hyperplasia, as well as the mechanism(s) responsible for reversion to a normal phenotype after AP20187 re-

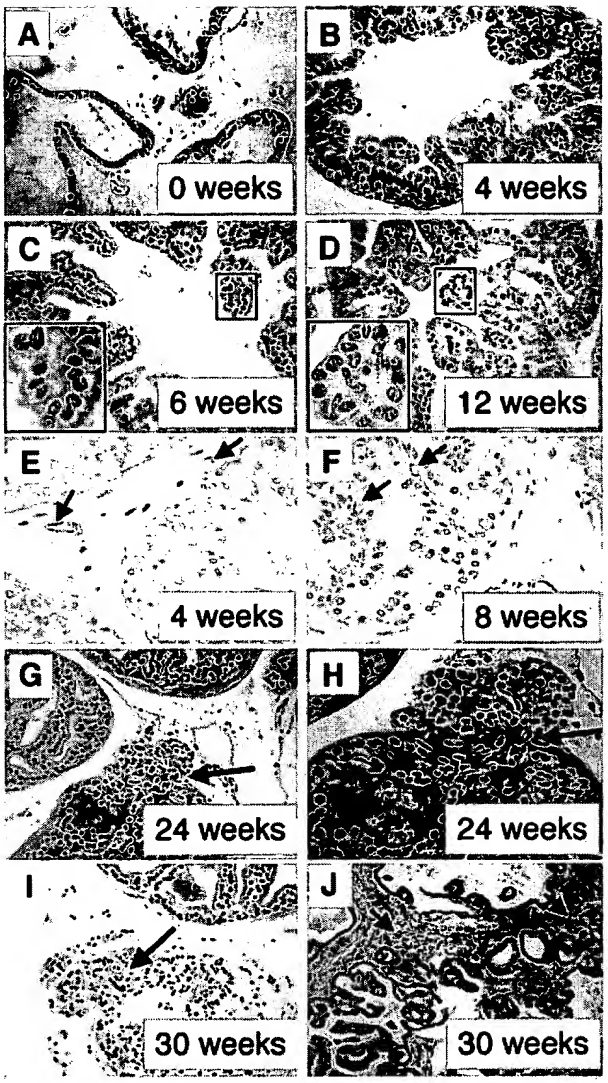

Fig. 3. Activation of iFGFR1 leads progressively to grade PIN IV in JOCK-1 animals. JOCK-1 mice were treated with diluent for 8 weeks (*A*) or with AP20187 for 4 (*B* and *E*), 6 (*C*), 8 (*F*), 12 (*D*), 24 (*G* and *H*), or 30 weeks (*I* and *J*). Paraffin sections from the ventral prostate (*A–F* and *J*) or dorsal-lateral prostate (*G–I*) were either H&E stained (*A–D* and *G–J*) or immunostained for vasculature with antibodies specific for CD31 (*E* and *F*), vasculature is indicated by *black arrows*. Herniated acini with cells extending into the stroma (*G–I*) or the presence of extensive reactive stroma (*J*) is indicated by *black arrows* Magnification = ×200 (*A-D, G, I,* and *inset*), ×400 (*E, F,* and *H*), ×100 (*J*).

moval. Staining for the proliferation marker, Ki-67, showed marked increases from 1% positive, observed in CID-treated wild-type or mock-treated transgenic mice, to 18% Ki-67-positive after 1 week of treatment (Fig. 5*A*). From 4 weeks of CID treatment onward, as cellular crowding in treated glands becomes widespread, Ki-67 staining stabilized at a lower level of ~ 8%. When treatment was stopped after 4 weeks of AP20187 administration, a gradual decrease in Ki-67 levels was observed with levels dropping to 1.5% by 2 weeks post-treatment and eventually reaching a minimum of 0.1% at week 4 before gradually returning to normal. Similarly, in mice administered CID for 8 weeks followed by 8 weeks of CID removal, Ki-67-positive staining eventually returned to normal levels, demonstrating that even after neovascularization, proliferation is still reversible (Fig. 5*A*; Fig. 4, *E versus F*).

To determine whether CID treatment or withdrawal led to quantifiable changes in the rate of apoptosis, we conducted terminal deoxynucleotidyl transferase-mediated nick end labeling staining analysis. Although levels of proliferation were below normal after CID removal, partially accounting for reversion to a normal glandular appearance, no obvious increase in terminal deoxynucleotidyl transferase-mediated nick end labeling staining was observed at 1, 2, 4, 6, and 8 weeks after CID withdrawal that could account more fully for the complete reversion seen 8 weeks after discontinuation of treatment (data not shown). Likely reasons for failing to observe increased apoptosis include: (*a*) the possibility that dying cells had been shed into the lumen and rapidly cleared; and (*b*) rapid and efficient phagocytosis by intraductal macrophages or other scavenging cells.

Erk Signaling Correlates with Hyperplasia and Progression. On the basis of prior *in vitro* studies of iFGFR1 signaling in TRAMP-derived iFGFR1-expressing cells, where we observed strong nuclear staining of p-Erk after iFGFR1 activation,[7] we hypothesized that the FGFR targets, Erk1/2, might also be involved in the observed changes in proliferation *in vivo*. Therefore, we examined Erk activation and localization by immunohistochemistry using p-ERK-specific antibodies. In untreated JOCK-1 glands (Fig. 5*B*), as well as in treated JOCK-2 mice (data not shown), we observed strong apical cytoplasmic staining of p-Erk in the majority of epithelial cells in the ventral lobe. In the other lobes of the prostate, p-ERK appeared diffuse or nuclear-localized and did not change with iFGFR1 activation (data not shown). However, after 1 week or more of CID treatment, we observed nuclear translocation of p-Erk in epithelial cells of the ventral lobe (Fig. 5*C*). When AP20187 was withheld for 8 weeks after 4 weeks of treatment, p-Erk gradually returned to its apical cytoplasmic position (Fig. 5*D*) corresponding to the loss of Ki-67 staining. Therefore, CID treatment leads to the reversible translocation of p-Erk from its polarized apical position to the nucleus.

We additionally conjectured that if CID-mediated nuclear accumulation of p-Erk was causative, translocation should precede proliferation. To additionally investigate this possibility, we performed immunohistochemistry for Ki-67 and p-Erk on serial sections from JOCK-1 mice treated with CID for 2, 6, 12, or 24 h. Whereas apical p-Erk staining was primarily observed at all of the time points, an increase in nuclear staining was seen from 2 h (Fig. 5*E*) to 24 h. Increased Ki-67 staining was not observed until 24 h (Fig. 5*F*). This suggests that signaling leads to nuclear accumulation of p-Erk, which precedes Ki-67-positive immunostaining. In contrast, JOCK-2 prostates, expressing iFGFR2, displayed no nuclear translocation of p-Erk even after 8 weeks of AP20187 administration, consistent with the lack of hyperplasia. Whereas we cannot explain the previously unreported, but consistent high-level apical staining of p-Erk, nuclear translocation correlates strongly with hyperplasia and progression.

DISCUSSION

Although the importance of FGFR1 and FGFR2 in CaP progression has been claimed frequently, published reports of the direct effects of these receptors within the context of a normal prostate gland are only beginning to be reported (20, 27). As an essential step toward better understanding the role of FGFRs in CaP progression, we have developed the first conditionally inducible and reversible CaP model, based on CID and FGFR1 signaling, called JOCK-1. The ability to control growth factor receptor signaling both spatially and temporally has both confirmed previous ideas that FGFR1 promotes CaP progression (28) and has led to new insights into how FGFR1 signaling affects the normal prostate epithelium. The JOCK-1 model demonstrates the dependence of CaP progression on continuous iFGFR1 signaling. This is shown by the reversibility of hyperplasia after early (4-week) CID removal and the termination of progression after later (8-week) CID

[7] K. W. Freeman and D. M. Spencer, unpublished observations.

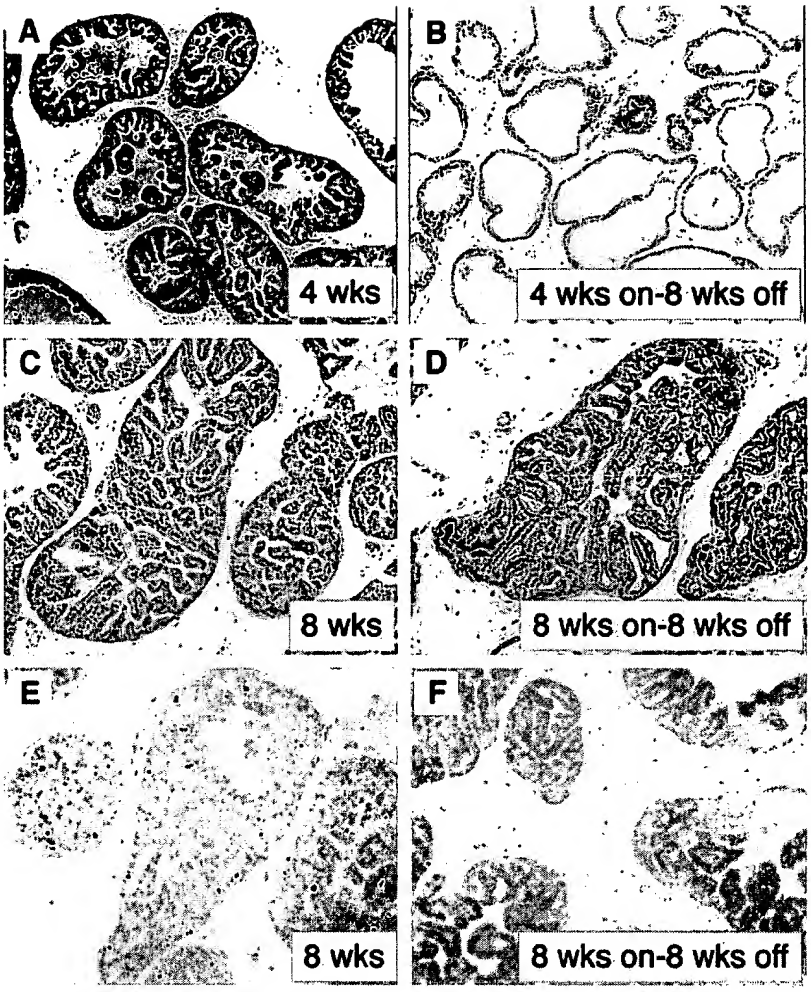

Fig. 4. JOCK-1 mice show reversible hyperplasia until established neovascularization. Paraffin sections of ventral prostates from JOCK-1 mice were H&E stained (*A–D*) or immunostained for proliferation with antibodies specific to Ki-67 (*E* and *F*) after treatment with AP20187 for 4 weeks (*A* and *B*) followed by AP20187 removal for 8 weeks (*B*) or treated with AP20187 for 8 weeks (*C–F*) followed by CID removal for 8 weeks (*D* and *F*).

removal. Additionally, FGFR1 signaling is necessary for both the initiation and maintenance of proliferation. In contrast, because detectable neovascularization trails hyperproliferation by several weeks, FGFR1 does not appear to directly stimulate angiogenesis, nor does CID removal lead to its reversal. Overall, in our model angiogenesis and stromal thickening appear to be secondary responses to increased epithelial cell numbers. This likely occurs via paracrine signaling from the epithelial cells and is not apparently due to the direct continuous action of iFGFR1 signaling, implying that the response of normal tissue (*e.g.,* increased vasculature) to pathological proliferation is not as reversible as the hyperproliferation itself.

The JOCK-1 model is reflective of what occurs during carcinogenesis when FGFR1, which is not expressed in adult epithelial cells, becomes expressed in the epithelial compartment. In contrast to FGFR1, FGFR2 signaling did not elicit observable changes in our model even after 12 weeks of CID treatment, consistent with a distinct role for FGFR2 in the normal prostate gland. Previously reported models overexpressing FGFR2-IIIb-binding FGFs (*i.e.,* FGF-3 or FGF-7) slowly develop mild hyperplasia. For example, overexpression of FGF-7 in the prostate, under the control of either mouse mammary tumor virus (18) or minimal probasin promoter (20), leads to hyperplasia after 9 months to a year. Whereas low transgene expression could account for the mild phenotype, an alternative explanation supported by our work is that FGFR2 signaling is insufficient for prostate transformation.

A similar hypothesis may explain the observed hyperproliferative effects of prostate-targeted FGF-3 also under the transcriptional control of the mouse mammary tumor virus promoter. In these mice, FGF-3 expression within the urogenital track led to extensive hyperplasia in all of the prostate glands (19), seemingly at odds with the inability of iFGFR2 to trigger hyperproliferation. However, unlike FGF-7, FGF-3 can also signal through other FGFRs, such as FGFR1-IIIb, which has been found in the tumor vasculature of TRAMP mice (29). Overexpression of FGF-8b, which signals through FGFR2-IIIc, FGFR3-IIIc, and FGFR4, also leads to the development of PIN (5), suggesting that activation of other FGF receptors besides FGFR1 can participate in CaP progression.

Unlike in our model where FGFR2 signaling is targeted to the epithelium, ectopic FGFs likely act as paracrine factors of which the direct effects are harder to pinpoint. Thus, our models help to clarify the unique roles for distinct FGFRs. In this regard, we observed differences previously in osteopontin production and Erk phosphorylation between iFGFR1 and iFGFR2 in TRAMP cell lines (30). Differential phosphorylation of FRS2, the major downstream substrate of FGFR, has also been observed between these two receptors (31). Together, this suggests that dissection of the signaling differences between iFGFR1 and iFGFR2 should illuminate new targets for therapeutic intervention.

JOCK-1 mice show highly reproducible pathological changes and attain grade PIN IV 3 months to a year earlier than in other single genetic lesion-based CaP models (2, 5, 25). Moreover, the effects of FGFR1 are highly penetrant, as 100% of JOCK-1 mice treated for as little as 12 weeks with AP20187 show PIN in virtually every acinus. Therefore, the JOCK-1 model should be ideal for studying the early

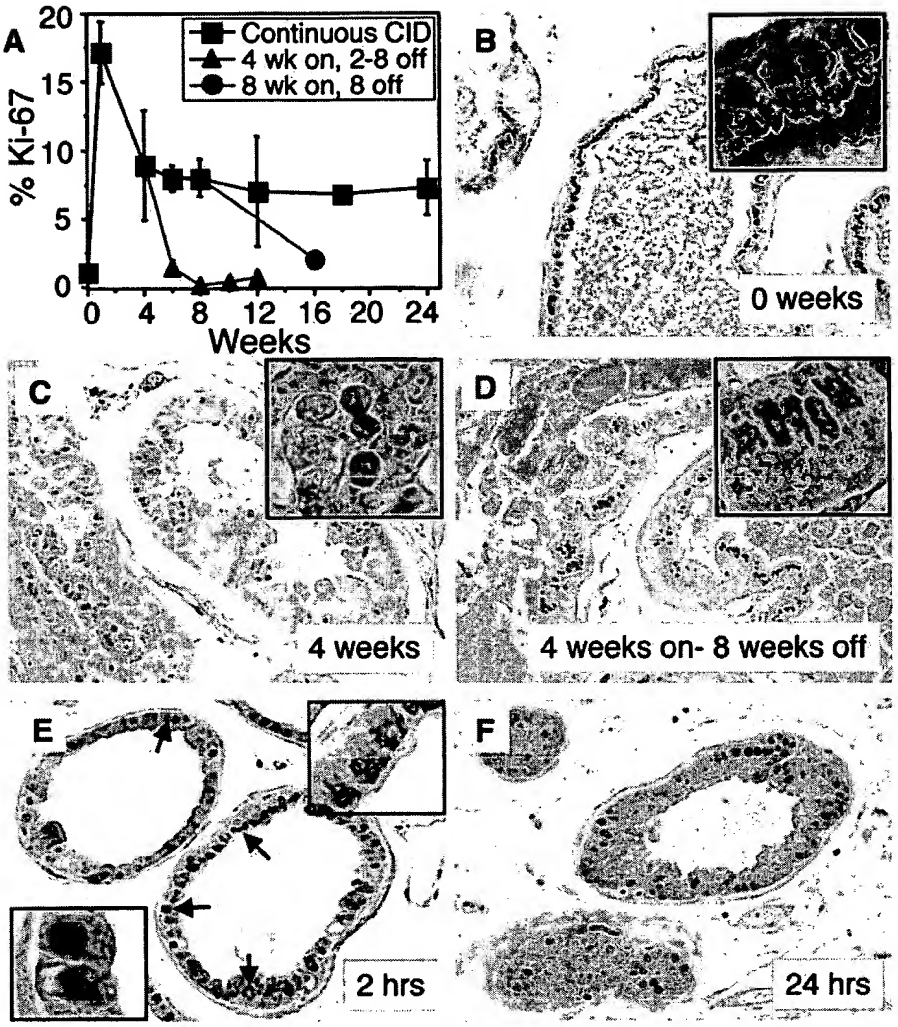

Fig. 5. In JOCK-1 mice, activation of iFGFR1 leads to iFGFR1-dependent hyperproliferation and reversible nuclear translocation of phosphorylated Erk that precedes proliferation. The percent of Ki-67 positive cells for at least 3 mice per time point (except t = 18 week) are summarized graphically (*A*). Paraffin sections of ventral prostates from JOCK-1 mice treated with diluent for 8 weeks (*B*), or with AP20187 for 2 h (*E*), 24 h (*F*), or AP20187 for 4 weeks (*C*) followed by CID removal for 8 weeks (*D*) were immunostained with antibodies to p-Erk (*B–E*) or Ki-67 (*F*). All panels are shown at ×200 with *insets* at ×400. *Black* and *red arrows* represent nuclear and apical p-Erk staining, respectively, with corresponding *insets* similarly color-coded (*E*).

stages of CaP and for testing early intervention strategies. Crossing JOCK-1 mice with other CaP susceptibility models may lead to metastatic CaP, providing novel metastatic CaP models as well. Finally, this approach can be easily adapted to virtually any cell surface receptor that is activated by cross-linking, a growing list that may even include G protein-coupled receptors (32).

ACKNOWLEDGMENTS

We thank Dr. Robert Cardiff for guidance on grading PIN lesions, Julie Zhao for expert technical assistance, Richard Cook for a careful reading of the manuscript, and members of the Spencer, Greenberg, and Rosen labs for helpful advice and discussions. AP20187 was a generous gift from ARIAD Pharmaceutical.[8]

REFERENCES

1. Jemal, A., Murray, T., Samuels, A., Ghafoor, A., Ward, E., and Thun, M. J. Cancer statistics, 2003. CA Cancer J. Clin., *53:* 5–26, 2003.
2. Abate-Shen, C., and Shen, M. M. Mouse models of prostate carcinogenesis. Trends Genet., *18:* S1–S5, 2002.
3. Greenberg, N. M., DeMayo, F., Finegold, M. J., Medina, D., Tilley, W. D., Aspinall, J. O., Cunha, G. R., Donjacour, A. A., Matusik, R. J., and Rosen, J. M. Prostate cancer in a transgenic mouse. Proc. Natl. Acad. Sci. USA, *92:* 3439–3443, 1995.
4. Masumori, N., Thomas, T. Z., Chaurand, P., Case, T., Paul, M., Kasper, S., Caprioli, R. M., Tsukamoto, T., Shappell, S. B., and Matusik, R. J. A probasin-large T antigen transgenic mouse line develops prostate adenocarcinoma and neuroendocrine carcinoma with metastatic potential. Cancer Res., *61:* 2239–2249, 2001.
5. Song, Z., Wu, X., Powell, W. C., Cardiff, R. D., Cohen, M. B., Tin, R. T., Matusik, R. J., Miller, G. J., and Roy-Burman, P. Fibroblast growth factor 8 isoform B overexpression in prostate epithelium: a new mouse model for prostatic intraepithelial neoplasia. Cancer Res., *62:* 5096–5105, 2002.
6. Podsypanina, K., Ellenson, L. H., Nemes, A., Gu, J., Tamura, M., Yamada, K. M., Cordon-Cardo, C., Catoretti, G., Fisher, P. E., and Parsons, R. Mutation of Pten/Mmac1 in mice causes neoplasia in multiple organ systems. Proc. Natl. Acad. Sci. USA, *96:* 1563–1568, 1999.
7. Gingrich, J. R., Barrios, R. J., Morton, R. A., Boyce, B. F., DeMayo, F. J., Finegold, M. J., Angelopoulou, R., Rosen, J. M., and Greenberg, N. M. Metastatic prostate cancer in a transgenic mouse. Cancer Res., *56:* 4096–4102, 1996.
8. Mentor-Marcel, R., Lamartiniere, C. A., Eltoum, I. E., Greenberg, N. M., and Elgavish, A. Genistein in the diet reduces the incidence of poorly differentiated prostatic adenocarcinoma in transgenic mice (TRAMP). Cancer Res., *61:* 6777–6782, 2001.
9. Foster, B. A., Kaplan, P. J., and Greenberg, N. M. Peptide growth factors and prostate cancer: new models, new opportunities. Cancer Metastasis Rev., *17:* 317–324, 1998.
10. Schlessinger, J., Plotnikov, A. N., Ibrahimi, O. A., Eliseenkova, A. V., Yeh, B. K., Yayon, A., Linhardt, R. J., and Mohammadi, M. Crystal structure of a ternary FGF-FGFR-heparin complex reveals a dual role for heparin in FGFR binding and dimerization. Mol. Cell., *6:* 743–750, 2000.
11. Spencer, D. M., Wandless, T. J., Schreiber, S. L., and Crabtree, G. R. Controlling signal transduction with synthetic ligands. Science (Wash. DC), *262:* 1019–1024, 1993.
12. Spencer, D. M., Graef, I., Austin, D. J., Schreiber, S. L., and Crabtree, G. R. A general strategy for producing conditional alleles of Src-like tyrosine kinases. Proc. Natl. Acad. Sci. USA, *92:* 9805–9809, 1995.
13. Blau, C. A., Peterson, K. R., Drachman, J. G., and Spencer, D. M. A proliferation switch for genetically modified cells. Proc. Natl. Acad. Sci. USA, *94:* 3076–3081, 1997.
14. MacCorkle, R. A., Freeman, K. W., and Spencer, D. M. Synthetic activation of caspases: artificial death switches. Proc. Natl. Acad. Sci. USA, *95:* 3655–3660, 1998.

[8] Internet address: http://www.ariad.com/regulationkits/.

15. Kaplan, P. J., Mohan, S., Cohen, P., Foster, B. A., and Greenberg, N. M. The insulin-like growth factor axis and prostate cancer: lessons from the transgenic adenocarcinoma of mouse prostate (TRAMP) model. Cancer Res., *59:* 2203–2209, 1999.
16. Ricol, D., Cappellen, D., El Marjou, A., Gil-Diez-de-Medina, S., Girault, J. M., Yoshida, T., Ferry, G., Tucker, G., Poupon, M. F., Chopin, D., Thiery, J. P., and Radvanyi, F. Tumour suppressive properties of fibroblast growth factor receptor 2-IIIb in human bladder cancer. Oncogene, *18:* 7234–7243, 1999.
17. Zhang, Y., Wang, H., Toratani, S., Sato, J. D., Kan, M., McKeehan, W. L., and Okamoto, T. Growth inhibition by keratinocyte growth factor receptor of human salivary adenocarcinoma cells through induction of differentiation and apoptosis. Proc. Natl. Acad. Sci. USA, *98:* 11336–11340, 2001.
18. Kitsberg, D. I., and Leder, P. Keratinocyte growth factor induces mammary and prostatic hyperplasia and mammary adenocarcinoma in transgenic mice. Oncogene, *13:* 2507–2515, 1996.
19. Chua, S. S., Ma, Z. Q., Gong, L., Lin, S. H., DeMayo, F. J., and Tsai, S. Y. Ectopic expression of FGF-3 results in abnormal prostate and Wolffian duct development. Oncogene, *21:* 1899–1908, 2002.
20. Foster, B. A., Evangelou, A., Gingrich, J. R., Kaplan, P. J., DeMayo, F., and Greenberg, N. M. Enforced expression of FGF-7 promotes epithelial hyperplasia whereas a dominant negative FGFR2iiib promotes the emergence of neuroendocrine phenotype in prostate glands of transgenic mice. Differentiation, *70:* 624–632, 2002.
21. Welm, B. E., Freeman, K. W., Chen, M., Contreras, A., Spencer, D. M., and Rosen, J. M. Inducible dimerization of FGFR1: development of a mouse model to analyze progressive transformation of the mammary gland. J. Cell Biol., *157:* 703–714, 2002.
22. Fan, L., Freeman, K. W., Khan, T., Pham, E., and Spencer, D. M. Improved artificial death switches based on caspases and FADD. Hum. Gene. Ther., *10:* 2273–2285, 1999.
23. Zhang, J., Thomas, T. Z., Kasper, S., and Matusik, R. J. A small composite probasin promoter confers high levels of prostate- specific gene expression through regulation by androgens and glucocorticoids *in vitro* and *in vivo*. Endocrinology, *141:* 4698–4710, 2000.
24. Wu, X., Wu, J., Huang, J., Powell, W. C., Zhang, J., Matusik, R. J., Sangiorgi, F. O., Maxson, R. E., Sucov, H. M., and Roy-Burman, P. Generation of a prostate epithelial cell-specific Cre transgenic mouse model for tissue-specific gene ablation. Mech. Dev., *101:* 61–69, 2001.
25. Park, J. H., Walls, J. E., Galvez, J. J., Kim, M., Abate-Shen, C., Shen, M. M., and Cardiff, R. D. Prostatic intraepithelial neoplasia in genetically engineered mice. Am. J. Pathol., *161:* 727–735, 2002.
26. Iuliucci, J. D., Oliver, S. D., Morley, S., Ward, C., Ward, J., Dalgarno, D., Clackson, T., and Berger, H. J. Intravenous safety and pharmacokinetics of a novel dimerizer drug, AP1903, in healthy volunteers. J. Clin. Pharmacol., *41:* 870–879, 2001.
27. Wang, F., McKeehan, K., Yu, C., Ittmann, M., and McKeehan, W. L. Chronic activity of ectopic type 1 fibroblst growth factor receptor tyrosine kinase in prostate epithelium results in hyperplasia accompanied by intraepithelial neoplasia. Prostate, in press, 2003.
28. Feng, S., Wang, F., Matsubara, A., Kan, M., and McKeehan, W. L. Fibroblast growth factor receptor 2 limits and receptor 1 accelerates tumorigenicity of prostate epithelial cells. Cancer Res., *57:* 5369–5378, 1997.
29. Huss, W. J., Barrios, R. J., Foster, B. A., and Greenberg, N. M. Differential expression of specific FGF ligand and receptor isoforms during angiogenesis associated with prostate cancer progression. Prostate, *54:* 8–16, 2003.
30. Freeman, K. W., Gangula, R. D., Welm, B. E., Ozen, M., Foster, B. A., Rosen, J. M., Ittmann, M., Greenberg, N. M., and Spencer, D. M. Conditional activation of fibroblast growth factor receptor (FGFR) 1, but not FGFR2, in prostate cancer cells leads to increased osteopontin induction, extracellular signal-regulated kinase activation, and *in vivo* proliferation. Cancer Res., *63*, 6237–6243, 2003.
31. Wang, F. Cell- and receptor isotype-specific phosphorylation of SNT1 by fibroblast growth factor receptor tyrosine kinases. In Vitro Cell Dev. Biol. Anim., *38:* 178–183, 2002.
32. Rios, C. D., Jordan, B. A., Gomes, I., and Devi, L. A. G-protein-coupled receptor dimerization: modulation of receptor function. Pharmacol. Ther., *92:* 71–87, 2001.